RSC Advances

PAPER

View Article Online
View Journal | View Issue

Cite this: *RSC Adv.*, 2017, **7**, 49883

Enhanced thermoelectric properties of $In_2O_3(ZnO)_5$ intrinsic superlattice ceramics by optimizing the sintering process

Li-Jun Cui, Zhen-Hua Ge,* Peng Qin and Jing Feng*

Received 5th June 2017
Accepted 16th October 2017

DOI: 10.1039/c7ra06267b

rsc.li/rsc-advances

Thermoelectric (TE) materials have a promising application as they can interconvert thermal energy to electrical energy directly. Oxide TE materials have attracted more attention for this application due to their high temperature stability. In this work, $In_2O_3(ZnO)_5$ intrinsic superlattice ceramics with a layered structure were synthesized by reaction sintering a mixed powder of In_2O_3 and ZnO at 1200 °C for different holding times (t = 6, 8, 10, 12 and 15 h) in air. Their thermoelectric properties including the electrical conductivity, Seebeck coefficient and thermal conductivity, were measured from 323 to 973 K. The thermoelectric properties depended on the holding time. The highest ZT value of 0.19 at 973 K was obtained for the sample with a 12 h holding time.

1. Introduction

Thermoelectric (TE) energy conversion has received more attention in the past decade on account of its promising application to directly convert waste heat into electricity.[1–4] This means that a huge amount of waste heat, including from human activities, can be converted into useful energy, helping to increase the production efficiency and improve living conditions. The TE figure-of-merit (ZT) is given by

$$ZT = \sigma\alpha^2 T/\kappa \quad (1)$$

where σ, α, T and κ are the electrical conductivity, the Seebeck coefficient, absolute temperature and the thermal conductivity, respectively.[5,6] According to the eqn (1), TE material which has good performance needs a large electrical conductivity, a Seebeck coefficient and a low thermal conductivity.

Semiconductor oxides are great prospective alternatives to conventional high temperature thermoelectric materials because of their high temperature stability and relatively wide bandgap. Currently, Si–Ge[7] alloy and $Yb_{14}MnSb_{11}$ (ref. 8) have high ZT value in high temperature, all of which possess problems such as high cost and toxic raw materials, especially Ge, Yb and Sb. BiCuSeO[9,10] maximum application temperature is 600 °C because of oxygen will disappear with the temperature increases. Therefore, the cheaper, high temperature stability and more environmental friendly TE materials are receiving increased attention.

ZnO has a wurtzite structure with space group $P6_3m$, belongs to the polar crystal classes.[11] It is pyroelectric and piezoelectric what represents the basis for applications in electromechanical or thermoelectric coupling devices. Moreover, ZnO which with a direct bandgap of 3.37 eV at room temperature is a semiconductor. In_2O_3 is also a wide bandgap transparent semiconductor ($E_g \approx 3.6$ eV) and has a high electrical conductivity.[12–15] Indium is sixfold coordinated in the In_2O_3 bixbyite structure, while zinc adopts fourfold coordination in the ZnO wurtzite structure.[16] The homologous compounds, $In_2O_3(ZnO)_k$ (k = integer), have very unique crystal structures with space groups of $R3m$ (for k = odd) or $P6_3/mmc$ (for k = even) and are composed of layers of $InO_{3/2}$, $InZnO_{5/2}$, and ZnO, what are stacked sequentially along the c-axis of the hexagonal system.[17,18] We can learn a lot from quite many previous studies on the inherent n-type behavior in In_2O_3 and ZnO.[19–23] The zincs disappear during the high temperature solid state reaction. So, the cation antisite defect, indium on zinc (InZn), also should be considered. V_O-Zn_i defect in ZnO and V_O-In_i in In_2O_3 for binaries are up to be the origin of n-type conductivity in un-doped ZnO and In_2O_3. $In_2O_3(ZnO)_5$ intrinsic superlattice ceramics have three advantages for application in thermoelectric materials. First of all, it possesses excellent structure and chemical stability even at high temperature (under 800 °C). Secondly its wide band gap prevents thermal excitation of "minor" carriers and thus allow the ZT increases at high temperature forward. For the layered structure, the carrier mobility along the layer direction is higher than that cross the layer direction. Thirdly, $In_2O_3(ZnO)_5$ has a very unique crystal structure composed of layers of InO_2^- and $InZn_5O_6^+$, periodically stacking in the c-axis direction. This layered structure gives rise to low thermal conductivity which is attributed to the reduced mean free path of the phonon between layers.

Faculty of Materials Science and Engineering, Kunming University of Science and Technology, Kunming 650093, China. E-mail: zge@kmust.edu.cn; jingfeng@kmust.edu.cn

In this work, the n-type $In_2O_3(ZnO)_5$ intrinsic superlattice ceramics were fabricated by a standard solid reaction 1200 °C for 6 h, 8 h, 10 h, 12 h and 15 h. There are $In_2Zn_7O_{10}$ impurity phase of 6 h, 8 h and 10 h. When the holding time is 15 h, the impurity phase appears in the sample and correspond well to $In_2Zn_4O_7$. Only the 12 h sample contain supreme *ZT* value of 0.19 at 973 K. We have found the best sintering process of $In_2O_3(ZnO)_5$. The resulting samples have an immense improvement over some other works.[45–50] This is a good foundation of further optimizing $In_2O_3(ZnO)_5$ thermoelectric performance in our next work.

2. Experiments

All samples, belonging to the $In_2O_3(ZnO)_k$ series, were prepared using a standard solid reaction route. Starting powders, In_2O_3 (Aladdin, 99.99%) and ZnO (Aladdin, 99.99%), were weighed in stoichiometric amounts and ground together by ball milling using agate balls and vial. The resulting powers were pressed uniaxially under 30 MPa, forming parallel disc with dimensions of 15 mm × 8 mm pellets. The pellets were transference into an alumina crucible and calcined at 1200 °C for 6–15 h.

The samples were characterized by X-ray diffraction (XRD: Cu-Kα Bruker D8, Germany) and the density (ρ) of the sample was determined by Archimedes method. The fractographs were measured by a scanning electron microscope (SEM, ZEISS, EVO 18-21-57).

The Seebeck coefficient and electrical resistance were measured using a Seebeck coefficient/electrical resistance measuring system (ZEM-3, Ulvac-Riko, Japan) in a He atmosphere (0.015 MPa pressure) which use the 2 × 2 × 8 mm cuboid sample. The Seebeck coefficient was calculated from thermoelectric voltage generated between both ends of a sample ΔV and temperature difference between the two ends ΔT. The thermal diffusivity (D) was measured by laser flash method (NETZSCH, LFA457, Germany) in flow argon atmosphere (80 ml min^{-1}) which requires that the samples are discs with a diameter of 6 mm. The electrical and thermal properties of the samples were tested perpendicular to pressure direction. The Hall coefficients (R_H) of the samples were measured at 293 K using a physical properties measurement system (HMS-7000), and a magnetic field of 2 T and electrical current of 30 mA were applied. The carrier concentration (n_i) was calculated by $n_i = 1/eR_H$, where e is the electronic charge. The carrier mobility (μ_i) was calculated by $\mu_i = R_H/\rho$. The thermal conductivity (κ) was calculated from the density (ρ), specific heat and thermal diffusivity using the relationship $\kappa = DC_p\rho$. These thermoelectric properties were measured in the temperature range of 323–973 K.

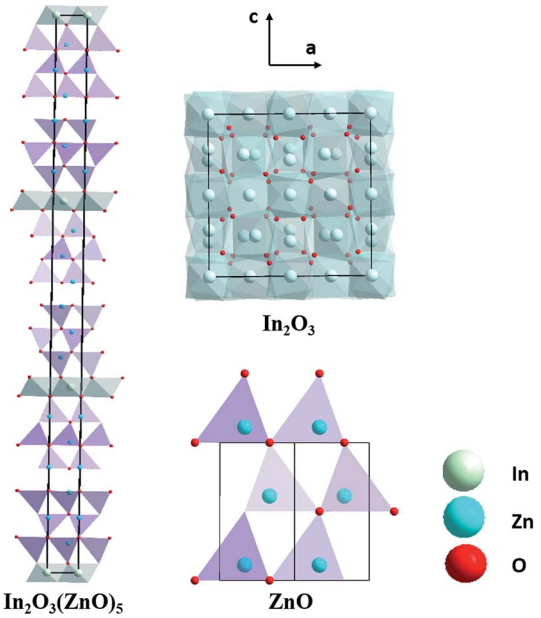

Fig. 1 Schematic representation of crystal structure from [010] direction for $In_2O_3(ZnO)_5$, parent oxides ZnO and In_2O_3 are also shown for comparison. Unit cells are marked by the black lines.

3. Result and discussion

3.1 Phase and microstructure

Fig. 1 shows the schematic representation of crystal structure from [010] direction for $In_2O_3(ZnO)_5$, parent oxides ZnO and In_2O_3 are also shown for comparison. Unit cells are marked by the blue lines. In the primitive cell of $In_2O_3(ZnO)_5$ has 150 atoms.[24] Both Zn and In atoms occupy the crystallographic positions. In other words, incorporation of In into ZnO slab is random, as is shown in the schematic representation of refined crystal structures (Fig. 1). In atomic ordered into the ZnO thin plate (*i.e.*, "zigzag fringe") has surveyed in previous studies and is thought to have a thermodynamic stability.[25–27] This structure what configuration of In in ZnO slab in our case can be obtained by high temperature calcinations which using a dilatory cooling

Table 1 The elemental mapping were performed for $In_2O_3(ZnO)_5$ with different holding time (t = 6, 8, 10, 12 and 15 h)

Bulk samples	Indium mass norm [%]	Zinc mass norm [%]	Oxygen mass norm [%]	Indium atom [%]	Zinc atom [%]	Oxygen atom [%]	Abs. error [%]	Rel. error [%]
6 h	81.32	79.21	9.47	49.15	9.77	41.08	2.64	22.33
8 h	40.19	49.35	10.46	16.65	40.89	42.46	3.55	16.09
10 h	37.97	50.65	11.38	15.72	37.17	47.11	3.12	17.12
12 h	33.04	49.79	17.17	13.02	34.58	47.94	2.16	9.18
15 h	24.48	54.95	20.57	9.11	35.92	54.97	3.98	15.89

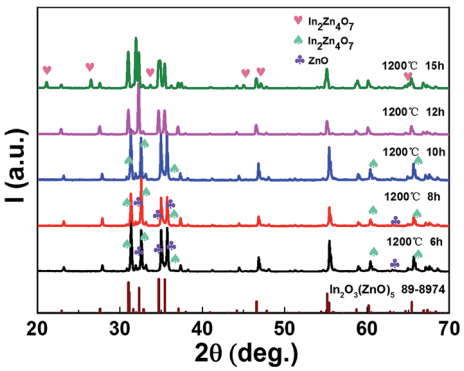

Fig. 2 Observed X-ray diffraction patterns of $In_2O_3(ZnO)_5$ at 1200 °C for 6–15 h holding time.

Table 2 The crystallinity of the samples sintered at different holding times (t = 6, 8, 10, 12 and 15 h)

Sample	6 h	8 h	10 h	12 h	15 h
Crystallinity (%)	86.30	88.19	89.27	91.45	89.83

rate (~5 °C). It is worthy to mention that the refined crystal structures of homologous compounds clearly indicate a close relationship to their parent oxides ZnO and In_2O_3.[28] According to their distinct coordination numbers (k), we can identify easily the layers of wurtzite type and bixbyite type structure. Wurtzite type structure similar with ZnO is largely maintained in these homologous compounds although deviation from the trigonal-bipyramidal coordination ($k = 5$) occurs.

As the data in Table 1 indicate, the content of In decreased with the increase of holding time. And the In atomic ratio is 49.15% in the $In_2O_3(ZnO)_5$ dispersed with 6 h, however, $In_2O_3(ZnO)_5$ dispersed with 15 h bulk sample In atomic ratio decreased to 9.11%. Because heating for longer time results into potential loss of indium. The $In_2O_3(ZnO)_5$ intrinsic superlattice ceramics were synthesized at 1200 °C for different holding time (6–15 h) as shown in Fig. 2. There are rhombohedral symmetry $In_2O_3(ZnO)_5$ of all specimens, which corresponds well to the PDF#89-8974 card.[29] These results are consistent with the previous reports that $In_2O_3(ZnO)_k$ crystallize in group $R3m$ for odd k values and $P6_3/mmc$ for even k values.[30–32] Heating for longer time brings about potential loss of indium and zinc. There are $In_2Zn_7O_{10}$ impurity phase in 6 h, 8 h and 10 h samples. In addition, there are ZnO impurity in the 6 h and 8 h sample. When the holding time is 15 h, the impurity phase appears in the sample and correspond well to $In_2Zn_4O_7$. Only the 12 h holding time sample is $In_2O_3(ZnO)_5$ pure phase. The crystallinity of all samples is showed in Table 2. As shown in Fig. 2, the peak intensity in 2θ ranges 30–47° for all the samples have obvious changes, indicating that there is texture in all the

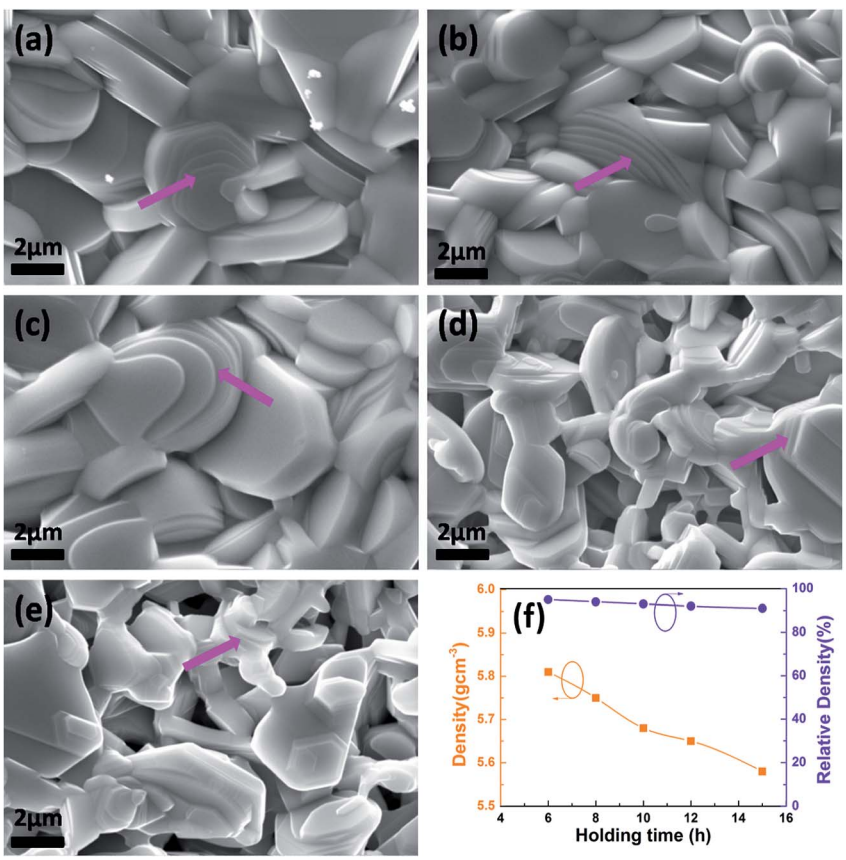

Fig. 3 The scanning electron microscopy images of $In_2O_3(ZnO)_5$ at 1200 °C for 6 h (a), 8 h (b), 10 h (c), 12 h (d), 15 h (e); the density and relative density of at $In_2O_3(ZnO)_5$ 1200 °C for 6–15 h (f).

samples. As the holding time is 15 h, the B of peaks increased, indicating the grain refinement according the Debye–Scherrer formula, $d = \frac{K\gamma}{B\cos\theta}$,[33] ($K$ is the Scherrer constant, d is the average thickness of the crystal grains perpendicular to the crystal plane direction, B is the diffraction width of the measured sample, θ is the diffraction angle, γ is the X-ray wavelength, 0.154056 nm).

Fig. 3 shows the scanning electron microscopy (SEM) images of $In_2O_3(ZnO)_5$ at 1200 °C for 6 h (a), 8 h (b), 10 h (c), 12 h (d), 15 h (e). From the Fig. 3 the grain distribution is relatively uniform. The powders were sintered to bulk at high temperature. The bulk samples have the large grain size of several micrometers. In other words, all the grains were observed with the sharp edge, and their layered structure was described in terraced fields (indicated by the purple arrow on the SEM images). The density of the samples shows the tendency of decreased with the increase of holding time, as is shown Fig. 3(f). It is because that as the extension of holding time from 6 h to 15 h, the $In_2O_3(ZnO)_5$ ceramic samples possess more and more pores because of potential loss of indium and zinc.

3.2 Thermoelectric properties

Fig. 4 shows that the temperature dependence of electrical transport properties for the $In_2O_3(ZnO)_5$ ceramics at 1200 °C for 6–15 h. The electrical conductivity (σ) of 6 h and 8 h samples increased with the increasing temperature, being indicative of the semiconductor behavior in Fig. 4(a). When the holding time is 10 h, 12 h or 15 h, which σ decreased with the increasing temperature, showed a metallic behavior. As H. Ohta *et al.*[43] research work shows that $In_2Zn_7O_{10}$ and $(ZnO)_5In_2O_3$ showed a metallic behavior and the pure ZnO showed a semiconductor behavior. Hence the 6 h and 8 h samples showed a metallic behavior, while the 10 h, 12 h and 15 h samples showed a semiconductor behavior. The concentration of conduction electrons is rather high and fixed in the present temperature range possibly. It is possibly induced by certain small deviations from stoichiometric compositions because the carrier concentration is determined by the valence control mechanism expressed as the following eqn (2),

$$InO_{1.5} = In_{Zn}^{\cdot} + e' + O_o^{\times} + \frac{1}{4}O_2(g) \quad (2)$$

The σ depends on both carrier concentration n and mobility μ as the following eqn (3),

$$\sigma = ne\mu \quad (3)$$

where e is the electronic charge. The sample for 12 h show higher electrical conductivity than other holding time samples. As reported in previous work,[43] the electrical conductivity of $In_2Zn_7O_{10}$ is lower than the $In_2O_3(ZnO)_5$. Hence the electrical conductivity of 6 h, 8 h and 10 h samples lower than the 12 h sample. The space group of $In_2Zn_4O_7$ is $P6_3/mmc$, which structure is different with $In_2Zn_4O_7$ and $In_2Zn_7O_{10}$. We infer the existence of $In_2Zn_4O_7$ led the lower electrical conductivity. The

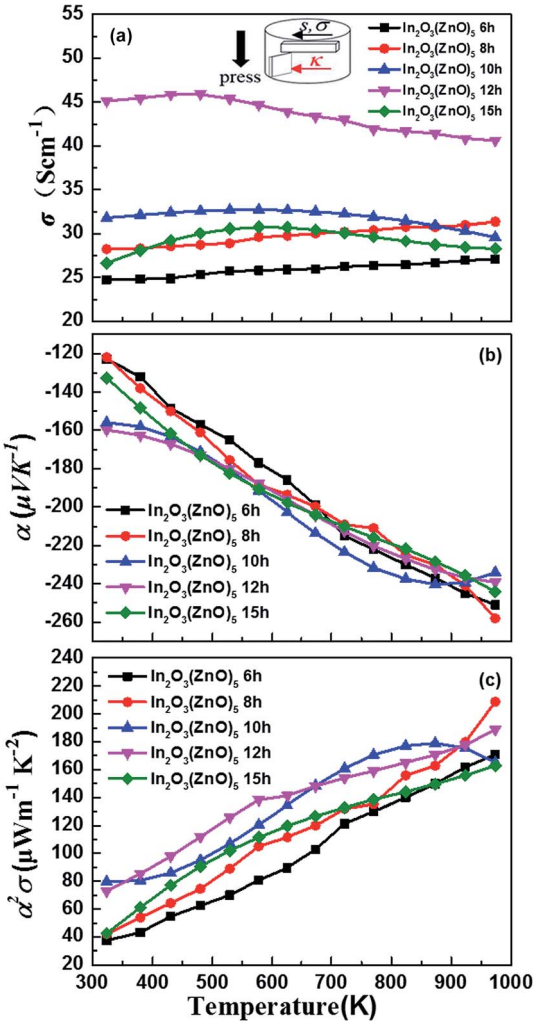

Fig. 4 The (a) temperature dependence of the electrical conductivity (σ), (b) the Seebeck coefficient (α), and (c) power factor ($\alpha^2\sigma$) for each bulk sample.

sample of 12 h has the highest electrical conductivity due to its pure $In_2O_3(ZnO)_5$ which has the noticeably higher density of the InO_2^- planar defects, representing highly conductive paths in the homologous phase. The holding time dependence of the carrier concentration (n_i) and the carrier mobility (μ_i) at room temperature has shown in Fig. 5. The extension of the holding time result into the potential loss of indium and zinc. Meanwhile indium substituted zinc and it produce electrons. Hence the carrier concentration increases with the extension of the holding time. The raised carrier concentration given rise to the reducing of carrier mobility in line with their calculation method. As shown in Fig. 4(b), the Seebeck coefficients (α) of all specimens were observed to be positive what account for ZnO–In_2O_3 ceramics are n-type semiconductor, meaning that the main carrier is electron. The absolute value of α increased with the increasing of temperature within the scope of the measuring temperature, which corresponding to the electrical conductivity. α is from the eqn (4) obtained,[34]

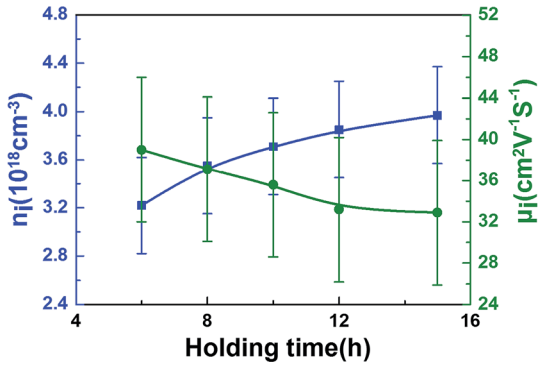

Fig. 5 The holding time dependence of the carrier concentration (n_i) and the carrier mobility (μ_i) at room temperature.

$$\alpha \approx \frac{2k_B^2}{e\hbar} m^* T\left(3\pi^2 n\right)^{-\frac{2}{3}} \quad (4)$$

where $\left(\frac{k_B}{e}\right)$ is the Seebeck coefficient for a classical electron gas. The different holding times make different carrier concentrations of the samples. The temperature dependence of power factor ($\sigma\alpha^2$) for $In_2O_3(ZnO)_5$ (1200 °C for 6–15 h) bulks is shown in Fig. 4(c). The material has high figure of merit who has large power factor. All the samples showed a similar positive temperature dependence of $\sigma\alpha^2$, despite having different slopes. With the increasing testing temperature, the power factor of the samples increased significantly because the Seebeck coefficient increased rapidly with temperature, and the power factor and the square of Seebeck coefficient were proportional. The maximum value of $\sigma\alpha^2$ of 209 μW m^{-1} K^{-2} was acquired for $In_2O_3(ZnO)_5$ (1200 °C, 8 h) at 973 K. In addition to $In_2O_3(ZnO)_5$ (1200 °C, 15 h), the $\sigma\alpha^2$ values of the specimens increased with increasing holding time.

Fig. 6(c) exhibits the temperature dependence of the total thermal conductivity (κ) for all bulk samples, what the κ value was calculated from the thermal diffusivity (D) (Fig. 6(a)), the heat capacity (C_p), the density (ρ), and $\kappa(\kappa = DC_p\rho)$. The κ decreased in the wake of holding time increasing. The thermal conductivity is presented by $\kappa = \kappa_c + \kappa_L$, κ_c is the thermal conductivity caused by electron transport and κ_L is the lattice thermal conductivity (Fig. 6(b)). κ_c is calculated by the Wiedemann Franz law, $\kappa_c = L\sigma T$, where L, σ and T are Lorenz number, electrical conductivity and absolute temperature, respectively. Reduced Fermi energy was used to calculate Lorenz number (eqn (5)) varies as Seebeck value changes (eqn (6)) with temperature or composition. The L calculation was estimated in a traditional single parabolic band model (resulting in an L with a deviation of less than 10% as compared with a more rigorous single non-parabolic band and multiple band models calculation) as described in ref. 35 and 36, where the reduced Fermi energy was implicitly determined by the Seebeck values (eqn (2)).

$$L = \left(\frac{k_B}{e}\right)^2 \left(\frac{(r+7/2)F_{r+5/2}(\eta)}{(r+3/2)F_{r+1/2}(\eta)} - \left[\frac{(r+5/2)F_{r+3/2}(\eta)}{(r+3/2)F_{r+1/2}(\eta)}\right]^2\right), \quad (5)$$

$$S = \pm\frac{k_B}{e}\left[\frac{(r+5/2)F_{r+3/2}(\eta)}{(r+3/2)F_{r+1/2}(\eta)} - \eta\right], \quad (6)$$

The difference in thermal conductivity is the contribution of the low relative density and anisotropic structure of $In_2O_3(ZnO)_5$. We assumed that interface scattering was generated by

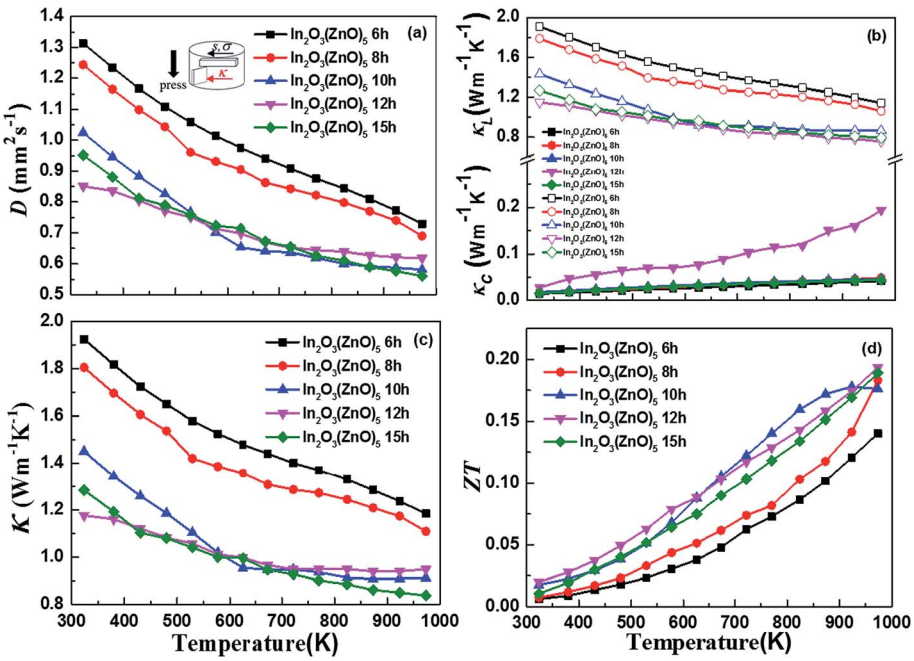

Fig. 6 The temperature dependence of thermal diffusivity (D) (a), the carrier thermal conductivity (κ_c) and the lattice thermal conductivity (κ_L) (b), the totally thermal conductivity (κ) (c) and ZT value (d) for all bulk samples.

porosity and difference in local density which arises from the anisotropic structure. One major perspective of nanostructure engineering to enhance thermoelectric properties is to design and create the (defect) structure with appropriate length scale, which is smaller than the mean free path of phonons but larger than that of electrons or holes.[37] The effect of superlattice structures on reducing thermal conductivity has been attributed to various mechanisms, including the modification of phonon spectrum,[38] phonon localizations, phonon scatterings at interfaces due to acoustic mismatch or defects formed arising from lattice mismatch[39] *etc.* It should be noted that phonon mean free path depends on both temperature and microstructural features, since temperature determines density of states of phonons and thereby affects phonon–phonon interactions/lattice imperfections introduce defect scatterings of phonons (eqn (7)).

$$\frac{1}{\iota_{\text{tot}}} = \frac{1}{\iota_{\text{ph-ph}}} + \sum \frac{1}{\iota_{\text{ph-def}}} \tag{7}$$

Assuming the scattering mechanisms are additive, the total phonon mean free path can be written as ref. 40. Superlattice belong to a surface defect. According to Zhao *et al.*,[41] its special layered structure introduces additional phonon scattering, reducing the mean free path of the phonon. Thereby the thermal conductivity of the samples is reduced. The values are agreement with the previous ones.[42,43] In addition to the κ value of all samples are very low and have a little reduction along with the increase of temperature. The total thermal conductivity trend consistent with the lattice thermal conductivity makes clear that κ_L occupies a leading position. The temperature dependence of the thermoelectric dimensionless figure of merit, *ZT*, is shown in Fig. 6(d). As shown in the eqn (8),[44]

$$ZT = \frac{\alpha^2 \sigma T}{\kappa} \tag{8}$$

The supreme *ZT* value of 0.19 was measured for the 12 h holding time sample at 973 K.

Fig. 7 shows the figure of merit of this work compared with other In_2O_3–ZnO system using different synthesis process. This work has an obvious improvement makes it an excellent candidate for further research and optimization for high-temperature thermoelectric applications.

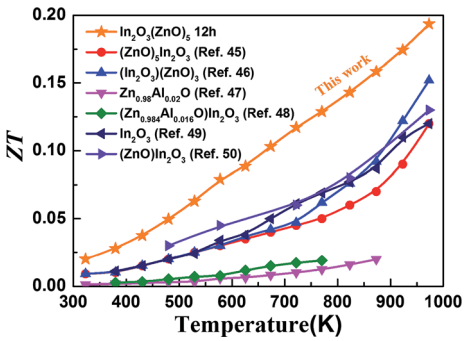

Fig. 7 The *ZT* value comparison of this work and other In_2O_3–ZnO system.

4. Conclusions

Intrinsic superlattice ceramics $In_2O_3(ZnO)_5$ with layered structures were synthesized by reaction sintering mixed powders of In_2O_3 and ZnO at 1200 °C for different holding time, $t = 6$, 8, 10, 12 and 15 h, in air. There are $In_2O_3(ZnO)_7$ impurity phase of 6 h, 8 h and 10 h samples. When the holding time is 15 h, the impurity phase appears in the sample and correspond well to $In_2O_3(ZnO)_4$. Only the 12 h holding time sample is $In_2O_3(ZnO)_5$ pure phase. They were dense and a number of stripes possibly corresponding to stacking faults were observed in every grain. This layered structure gives rise to low thermal conductivity due to it is attributed to the reduced mean free path of the phonon between layers. The thermoelectric *ZT* increasing with increasing temperature and holding time (6–12 h) with the exception of 15 h. The maximum figure of merit of 0.19 was detected for the 12 h holding time sample at 973 K. $In_2O_3(ZnO)_5$ intrinsic superlattice ceramics were found be the huge potential candidates materials for high temperature thermoelectric energy conversion.

Conflicts of interest

There are no conflicts to declare.

Acknowledgements

This work was supported by the National Natural Science Foundation of China (Grant No. 51501086) and Yunnan Provincial Natural Science Key Fund (Grant No. 2017FA023).

References

1 G. J. Snyder and E. S. Toberer, *Nat. Mater.*, 2008, **7**, 105.
2 M. G. Kanatzidis, *Chem. Mater.*, 2010, **22**, 648.
3 J. F. Li, W. S. Liu, L. D. Zhao and M. Zhou, *NPG Asia Mater.*, 2010, **2**, 152.
4 T. Moriga, K. Ishida and K. Yamamoto, *Mater. Res. Innovations*, 2009, **13**, 348–351.
5 G. S. Nolas, *Thermoelectrics: Basic Principles and New Materials Developments*, Springer, New York, 2001.
6 X. Liang, *J. Eur. Ceram. Soc.*, 2016, **36**, 1643–1650.
7 A. Usenko, D. Moskovskikh, M. Gorshenkov, A. Voronin, A. Stepashkin, S. Kaloshkin and V. Khovaylo, *Scr. Mater.*, 2017, **127**, 63–67.
8 S. R. Brown, S. M. Kauzlarich, F. Gascoin and G. J. Snyder, *Chem. Mater.*, 2006, **18**, 1873–1877.
9 L. D. Zhao, D. Berardan, Y. L. Pei, C. Byl, L. Pinsard-Gaudart and N. Dragoe, *Appl. Phys. Lett.*, 2010, **97**, 092118.
10 Y. Sun, C. Zhang, C. Cao, J. Fu and L. Peng, *J. Electron. Mater.*, 2017, 1–7.
11 R. D. Shannon, J. L. Gilson and R. J. Bouchard, *J. Phys. Chem. Solids*, 1997, **38**, 877–881.

12 C. Lizandara-Pueyo, S. Siroky, S. Landsmann, M. W. E. van den Berg, M. R. Wagner, J. S. Reparaz, A. Hoffmann and S. Polarz, *Chem. Mater.*, 2010, **22**, 4263.
13 C. G. Granqvist, Transparent conductive electrodes for electrochromic devices: a review, *Appl. Phys. A*, 1993, **57**, 19.
14 I. Hamburg and C. G. Granqvist, *Appl. Phys.*, 1986, **60**, 123.
15 C. Li, D. H. Zhang, X. L. Liu, S. Han, T. Tang, J. Han and C. W. Zhou, *Appl. Phys. Lett.*, 2003, **82**, 1613.
16 S. Yang, F. Chen, Q. Shen and L. Zhang, *J. Eur. Ceram. Soc.*, 2016, **36**, 1953–1959.
17 A. Walsh, J. L. F. Da Silva, Y. Yan, M. M. al-Jassim and Su-H. Wei, *Phys. Rev. B: Condens. Matter Mater. Phys.*, 2009, **79**, 073105.
18 O. Malochkin, W.-S. Seo and K. Koumoto, *Thermoelectric Properties of $(ZnO)_5In_2O_3$ Single Crystal Grown by a Flux Method*, Department of Applied Chemistry, Nsagoya 464-8603, Japan, 2004.
19 X. Liang, M. Baram and D. R. Clarke, *Appl. Phys. Lett.*, 2013, **102**, 223903.
20 S. B. Zhang, S. H. Wei and A. Zunger, *Phys. Lett. A*, 2001, **67**, 075205.
21 A. Janotti and C. G. Van de Walle, *Appl. Phys. Lett.*, 2005, **87**, 122102.
22 S. Lany, J. Osorio-Guillén and A. Zunger, *Phys. Rev. B: Condens. Matter Mater. Phys.*, 2007, **75**, 241203.
23 S. Lany and A. Zunger, *Phys. Lett. A*, 2007, **98**, 045501.
24 F. Oba, A. Togo, I. Tanaka, J. Paier and G. Kresse, *Phys. Rev. B: Condens. Matter Mater. Phys.*, 2008, **77**, 245202.
25 X. Zhang, H. Lu, H. Gao, X. J. Wang, H. Y. Xu, Q. Li and S. K. Hark, *Cryst. Growth Des.*, 2009, **9**, 364–367.
26 J. L. F. Da Silva, Y. F. Yan and S. H. Wei, *Phys. Rev. Lett.*, 2008, **100**, 255501.
27 C. F. Li, Y. Bando, M. Nakamura, M. Onoda and N. J. Kimizuka, *Solid State Chem.*, 1998, **139**, 347–355.
28 A. P. Goldstein, S. C. Andrews, R. F. Berger, V. R. Radmilovic, J. B. Neaton and P. D. Yang, *ACS Nano*, 2013, **7**, 10747–10751.
29 P. J. Cannard and R. J. D. Tilley, *J. Solid State Chem.*, 1988, **73**, 418–429.
30 W. Pitschke and K. Koumoto, Powder diffraction data and Rietveld refinement for Y-doped $(ZnO)_5In_2O_3$, *Powder Diffr.*, 1999, **14**, 213–218.
31 T. Moriga, D. D. Edwards, T. O. Mason, G. B. Palmer, K. R. Poeppelmeier, J. L. Schindler, C. R. Kannewurf and I. Nakabayashi, *J. Am. Ceram. Soc.*, 1998, **81**, 1310–1316.
32 A. Yoshinari, K. Ishida, K. I. Murai and T. Moriga, *Mater. Res. Bull.*, 2009, **44**, 432–436.
33 H. P. Klug and L. E. Alexander, *X-ray diffraction procedures [M]*, Wiley, New York, 1954, vol. 2.
34 G. J. Snyder and E. S. Toberer, Complex thermoelectric materials, *Nat. Mater.*, 2008, **7**, 105–114.
35 A. Greiner, L. Reggiani, T. Kuhn and L. Varani, *Phys. Rev. Lett.*, 1997, **78**, 1114.
36 H. S. Kim, Z. M. Gibbs, Y. Tang, H. Wang and G. J. Snyder, *APL Mater.*, 2015, **3**, 041506.
37 A. Majumdar, *Science*, 2004, **303**, 777–778.
38 V. Narayanamurti, *Phys. Rev. Lett.*, 1979, **43**, 2012–2016.
39 G. Chen, Phonon transport in low-dimensional structures, in *Recent Trends in Thermoelectric Materials Research Iii*, ed. T. M. Tritt, 2001, pp. 203–259.
40 G. Grimvall, *Thermalphysical Properties of Materials*, Amsterdam, North Holland, 1999.
41 L. D. Zhao, J. He, D. Berardan, Y. Lin, J. F. Li, C. W. Nan and N. Dragoe, *Energy Environ. Sci.*, 2014, **7**, 2900.
42 Y. Masuda, M. Otha, W. S. Seo, W. Pitschke and K. Koumoto, *J. Solid State Chem.*, 2000, **150**, 221–227.
43 H. Ohta, W. S. Seo and K. Koumoto, *J. Am. Ceram. Soc.*, 1996, **79**, 2193–2196.
44 M. Othtaki, K. Araki and K. Yamamoto, *J. Electron. Mater.*, 2009, **38**, 1234–1238.
45 M. Amani, I. M. Tougas, O. J. Gregory and G. C. Fralick, *J. Electron. Mater.*, 2013, **42**, 114–120.
46 Z. Materijala, *Zast. Mater.*, 2016, **57**, 318–325.
47 C. Dreßler, R. Löhnert, J. Gonzalez-Julian, O. Guillon, J. Töpfer and S. Teichert, *J. Electron. Mater.*, 2016, **45**, 1459–1463.
48 T. Endo, J. Fukushima, Y. Hayashi and H. Takizawa, *J. Ceram. Soc. Jpn.*, 2013, **121**, 416–421.
49 Y. Liu, Y. H. Lin, W. Xu, B. Cheng, J. Lan, D. Chen and C. W. Nan, *J. Am. Ceram. Soc.*, 2012, **95**, 2568–2572.
50 H. Kaga, A. Ryoji and T. Toshihiko, *Jpn. J. Appl. Phys.*, 2004, **43**(10), 7133.